Desalination and Water Treatment
www.deswater.com
2 (2009) 295–309
1944-3994/1944-3986

A mathematical tool for describing the behaviour of a dense effluent discharge

Andrea Cipollina*, Alberto Brucato, Giorgio Micale

Dipartimento di Ingegneria Chimica dei Processi e dei Materiali, Università di Palermo, Viale delle Scienze Ed.6, 90128 Palermo, Italy
Tel. +39 091 2386 3780; Fax. +39 091 2386 3750; email: cipollina@dicpm.unipa.it

Received 18 April 2008; Accepted 27 November 2008

ABSTRACT

In many cases a dense effluent has to be discharged in the environment with possible harmful consequences. The preferred design for the relevant discharge unit is that of a simple or multi-port diffuser issuing jets at a given inclination above the horizontal. This work presents the follow-on developments of a model previously proposed to predict the behaviour of inclined dense jets issuing in a stagnant environment. It consists of a set of three ordinary differential equations that can be solved by standard numerical methods. Model outputs include information on the trajectory, spreading and dilution of inclined dense jets, return point position and concentration. Interestingly the model also predicts velocities along the trajectory and values of return point velocity which can be of great importance in the design and monitoring of dense effluents diffusers. Model predictions are compared with experimental data from several sources and in all cases a good agreement is found. For user convenience, model implementations in the form of an Excel® spreadsheet or Matlab® routine have been made available as open access material upon request to the authors. Finally, dimensional analysis considerations are made that enlighten the use of the densimetric Froude number as the major, though not the sole, correlating parameter for dense jet behaviour.

Keywords: Dense effluents; Modelling; Inclined dense jets; Diffusers design tool; Return point dilution; Return velocity

1. Introduction

During the last 20 years, the sources of salty effluents to be discharged in water bodies have been steadily rising due to the increase in industrial activities producing such wastewaters as, among all, desalination plants. The current environmental sustainability policy adopted in most of industrial activities has boosted the attention towards the effects of such brine discharges into the sea [1]. Given the peculiar features of dense effluent discharges, which present a negatively buoyant behaviour, a proper reduction of harmful effects of the discharge can be achieved by means of diffusers properly designed in order to get the largest dilution before the impingement at the impact point, so avoiding the formation of a "salty desert" on the sea floor [2].

It is worth mentioning that dense jets issuing in a stagnant environment may also be frequently encountered in industrial mixing processes when jet-mixing is adopted, or in atmospheric pollutants dispersions when a heavy gas is issued in the form of a dense jet into stagnant air. Open technical and scientific literature offers several works on vertical dense jets issuing in stagnant liquids [3–6] or in the presence of a crosscurrent [5,7,8]. Fewer works report information on the behaviour of inclined dense jets [5,8–10], despite that they have long been known to result in larger dilution levels than vertical ones and are therefore preferable for the purpose of effluent dispersion [11].

*Corresponding author.

As concerns the availability of mathematical tools for predicting the behaviour of a brine discharge, several empirical correlations have been proposed [5,9–11], along with simplified models for predicting some of the geometrical and dilution parameters of negatively buoyant inclined jets [12–14]. An interesting integral model has been recently presented by Jirka [15] for the prediction of the behaviour of generally buoyant jets, able to account for the possible presence of cross flows. The model is well presented and structured, and comparison with experiments is good in most cases. However, the numerical implementation of the model is not presented and technical readers could find more comfortable the use of a ready-to-use model as that presented in this work, especially if the information needed is just a rough estimate of the jet dilution behaviour.

In the present work a previously proposed model for buoyant jets issuing in a stagnant environment [13] is further developed and validated. Among the other models presented in the literature, the present formulation provides significant advantages in terms of simplicity of implementation and availability of the open source files, which provide an easy-to -use tool for predicting in a comprehensive way all features of practical interest of inclined dense jets, like jet trajectory, velocities and dilution levels at any point, including the return point of the plume. In particular, prediction of velocities is another feature of the present model which is often neglected in other formulations available, although this last parameter can be of significant importance for the design and monitoring of dense effluent diffusers.

In practice, all the parameters needed for design purposes, including those required to recognise the possible need of protection measures against sea-floor erosion, are easily and reliably predicted.

2. Model description

2.1. Problem definition and simplifying assumptions

The development of a mathematical model for inclined dense jets has been carried out aiming at the widest range of applicability. Consequently simplifying hypothesis are quite general and based on the analysis of physical phenomena as they occur. A sketch of an inclined dense jet is shown in Fig. 1. The assumptions are:

1. The entrainment velocity is supposed to be simply proportional to the local velocity at jet axis [12,16], i.e.:

$$U_e = E \cdot u_{\max} = I \cdot u_m \tag{1}$$

where U_e is the entrainment velocity defined as the ratio dQ_e/dS where dS is the infinitesimal lateral surface, E is a suitable entrainment coefficient whereas I ($=E \cdot u_{\max}/u_m$) is the proportionality coefficient between U_e and the local mean velocity u_m.

2. Local jet density is computed on the basis of the local volumetric fraction ϕ of the discharged stream:

$$\rho = \rho_a + \phi(\rho_j - \rho_a) \tag{2}$$

where ρ_a and ρ_j are ambient and discharged stream densities respectively. Clearly Eq. (2) implies the assumption that volumetric mixing effects are negligible.

It is worth noting that the density difference between issuing jet and the ambient fluid may stem from temperature difference, composition difference, or both. All theses cases are dealt with by the present model.

3. Velocity and issuing jet volumetric fraction distributions around the jet axis are supposed to be Gaussian:

$$u(r) = u_{\max} e^{-A\left(\frac{r}{R}\right)^2} \tag{3}$$

$$\phi(r) = \phi_{\max} \cdot e^{-B\left(\frac{r}{R}\right)^2} \tag{4}$$

where r is the radial distance from the axis, A and B are non-dimensional coefficients, $u(r)$ and $u_{\max}$ are the local and the centreline velocity respectively, while $\phi(r)$ and $\phi_{\max}$ are the local and the centreline jet volumetric fraction respectively. R is assumed to be the jet radius and represents the conventional boundary limit of the jet. In the present model formulation, it is assumed to be twice the half radius (defined as the distance at which the local fluid velocity is 50% of the velocity at the centreline), i.e. the distance at which velocity is only 6% of centreline velocity.

The value for A is actually imposed by the above definition of R. Assuming that, at $r = R/2$, $u(r)$ is equal to $u_{\max}/2$, then A value must be equal to 2.77. B is assumed to be related to A according to the following relation, $B = A/1.17^2$ (= 2.025 in the present case), as suggested by Rajaratnam [16], underlining a width of the scalar property distribution larger than for the velocity.

Notably among the many bell-shaped curves which may describe transversal profiles of jet velocity and concentration, the Gaussian curve is practically universally adopted [14–17]. It is worth noting that the choice of constant values for A and B and the assumption of a Gaussian distribution of velocities and volumetric fractions can be considered as restrictive assumptions, in particular when large density differences characterize the jet. In fact, a distortion of profiles is generated by the intrinsic instability of the jet lower boundary due to

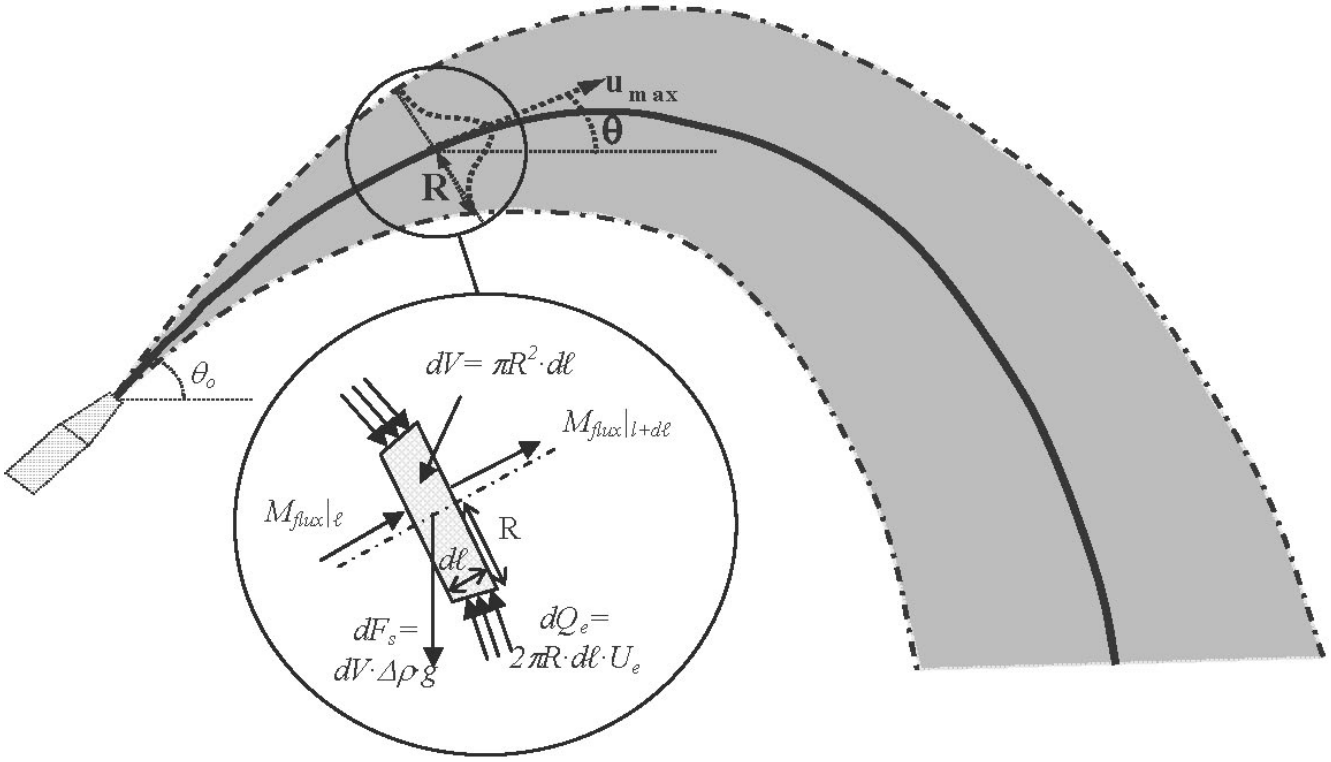

Fig. 1. Sketch of an inclined dense jet.

gravity forces [14]. Moreover the shape of the distribution can vary passing from the jet-like initial part of the discharge to the plume-like falling part of the discharge. On the other side, the choice of mean variables in the formulation of the model helps in reducing the overall dependence on velocity and concentration radial distributions. Therefore, the influence of the above assumption will probably be more significant in the calculation of axial variables from mean ones.

4. Turbulent momentum exchanges across the lateral surface of the jet are neglected in the momentum balance equation.

2.2. Governing equations

The model is based on the mass and momentum balances written for the infinitesimal volume $dV = \pi R^2 d\ell$ shown in Fig. 1, and on an integral mass balance written for the jet fluid between the nozzle issuing section and the local jet section at distance ℓ along the trajectory. The vector momentum equation is split into a horizontal scalar component and a vertical one, with the gravity force obviously present in the latter, due to the negatively buoyant behaviour of the effluent.

- Continuity equation (overall mass balance):

$$\left(\rho_{bm}\cdot\pi R^2\cdot u_m\right)_\ell-\left(\rho_{bm}\cdot\pi R^2\cdot u_m\right)_{\ell+d\ell}=-2\pi R\cdot d\ell\cdot\rho_a\cdot U_e \quad (5)$$

- Momentum flux, horizontal direction:

$$\left\{\pi R^2\left[\rho_a\lambda_{av}+\phi_{bm}\lambda_{bv}\left(\rho_j-\rho_a\right)\right]u_m^2\cos\theta\right\}_\ell -\left\{\pi R^2\left[\rho_a\lambda_{av}+\phi_{bm}\lambda_{bv}\left(\rho_j-\rho_a\right)\right]u_m^2\cos\theta\right\}_{\ell+d\ell}=0 \quad (6)$$

- Momentum flux, vertical direction:

$$\left\{\pi R^2\left[\rho_a\lambda_{av}+\phi_{bm}\lambda_{bv}\left(\rho_j-\rho_a\right)\right]u_m^2\sin\theta\right\}_\ell -\left\{\pi R^2\left[\rho_a\lambda_{av}+\phi_{bm}\lambda_{bv}\left(\rho_j-\rho_a\right)\right]u_m^2\sin\theta\right\}_{\ell+d\ell} =\pi R^2(\rho_m-\rho_a)g\,d\ell \quad (7)$$

- Integral jet fluid mass balance:

$$Q_o\rho_j=\left(\pi R^2\phi_{bm}\rho_j u_m\right)_\ell \quad (8)$$

The main variables are therefore the local jet radius R, the local jet trajectory inclination ϕ, the local mean velocity u_m [defined by Eq. (9)], the local volume mean density ρ_m [Eq. (10)], the local bulk mean density ρ_{bm} and the local bulk mean volumetric fraction ϕ_{bm} [Eqs. (11) and (12), respectively), whereas ℓ is the linear coordinate along the jet centreline. Coefficients λ_{av} and λ_{bv} are

defined by Eqs. (14) and (15) and allow the use of mean variables in Eqs. (6) and (7).

The analytical definitions of the above adopted variables and their operational form are shown below.

- u_m is the mean velocity across the jet section, i.e., the ratio between the overall volumetric flow rate and the jet cross section (πR^2), defined as:

$$u_m \equiv \frac{1}{\pi R^2}\cdot\int_0^R u(r)\cdot 2\pi\cdot r\cdot \mathrm{d}r = \frac{1}{\pi R^2}\cdot\int_0^R u_{\max}\cdot \exp[-A\cdot(r/R)^2]2\pi\cdot r\cdot \mathrm{d}r = u_{\max}\cdot\frac{1}{A}\cdot\left(1-e^{-A}\right) \quad (9)$$

- ρ_m is the local volume mean density, used for calculating the mean sinking force on the control volume $\mathrm{d}V$:

$$\rho_m-\rho_a=\phi_m\left(\rho_j-\rho_a\right)=\frac{1}{\pi R^2}\cdot\int_0^R[\rho(r)-\rho_a]\cdot 2\pi r\cdot \mathrm{d}r = \frac{1}{\pi R^2}\cdot\int_0^R\left(\rho_j-\rho_a\right)\cdot\phi_{\max}\cdot e^{-B\left(\frac{r}{R}\right)^2}\cdot 2\pi\cdot r\cdot \mathrm{d}r = \left(\rho_j-\rho_a\right)\cdot\phi_{\max}\frac{1}{B}\cdot\left(1-e^{-B}\right) \quad (10)$$

where ϕ_m is the mean jet concentration calculated within the infinitesimal volume $\mathrm{d}V = \pi R^2 \mathrm{d}\ell$.

The group $\phi_m\cdot\rho_j\cdot\mathrm{d}V$ gives the total mass of jet fluid in the control volume, directly related to the negative buoyancy force in Eq. (7).

ρ_{bm} is the mean bulk jet density, which can be multiplied by the mean velocity u_m to obtain the mass flux through the jet cross section (πR^2). Its definition, along with that of ϕ_{bm}, follows from the following considerations:

$$\rho_{bm}\cdot u_m\cdot\pi R^2=\int_0^R\rho(r)\cdot u(r)\cdot 2\pi\cdot r\cdot \mathrm{d}r = \int_0^R\left[\rho_a+\phi(r)\left(\rho_j-\rho_a\right)\right]\cdot u_{\max}\cdot e^{-A(r/R)^2}\cdot 2\pi\cdot r\mathrm{d}r = \rho_a\cdot u_m\cdot\pi R^2+\left(\rho_j-\rho_a\right)\cdot\phi_{bm}\cdot u_m\cdot\pi R^2 \quad (11)$$

with ϕ_{bm} being:

$$\phi_{bm}=\frac{1}{u_m\cdot\pi R^2}\cdot\int_0^R\phi(r)\cdot u(r)\cdot 2\pi\cdot r\mathrm{d}r = \frac{\phi_{\max}\cdot u_{\max}}{(A+B)\cdot u_m}\cdot\left[1-e^{-(A+B)}\right]=\frac{\phi_{\max}\cdot A}{(A+B)}\cdot\frac{1-e^{-(A+B)}}{1-e^{-A}} \quad (12)$$

The two coefficients λ_{av} and λ_{bv}, used in Eqs. (6) and (7), are purposely inserted to express the momentum flux by means of mean variables. This comes from imposing the equality between the momentum flux in terms of mean variables [LHS Eq. (13a)] and its corresponding integral form [RHS Eq. (13a)]:

$$\pi R^2\left[\rho_a\lambda_{av}+\phi_{bm}\lambda_{bv}\left(\rho_j-\rho_a\right)\right]u_m^2 = \int_0^R\rho(r)\cdot u^2(r)\cdot 2\pi\cdot r\mathrm{d}r \quad (13a)$$

where the RHS is further developed into the following form:

$$\int_0^R\rho(r)\cdot u^2(r)\cdot 2\pi\cdot r\,dr=\int_0^R\left[\rho_a+\phi(r)\cdot\left(\rho_j-\rho_a\right)\right]\cdot u^2(r)\cdot 2\pi\cdot r\mathrm{d}r = \int_0^R\rho_a\cdot u^2(r)\cdot 2\pi\cdot r\,dr+\int_0^R\phi(r)\cdot\left(\rho_j-\rho_a\right)\cdot u^2(r)\cdot 2\pi\cdot r\mathrm{d}r = \pi R^2\cdot\rho_a\cdot u_m^2\cdot\frac{\mathrm{A}}{2}\cdot\frac{1-e^{-2\mathrm{A}}}{\left(1-e^{-\mathrm{A}}\right)^2}+\pi R^2\phi_{bm}\cdot\left(\rho_j-\rho_a\right) \quad (13b)$$

$$\cdot u_m^2\cdot\frac{\mathrm{A}\cdot(\mathrm{A}+\mathrm{B})}{(2\,\mathrm{A}+\mathrm{B})}\cdot\frac{1-e^{-(2\mathrm{A}+\mathrm{B})}}{\left(1-e^{-(\mathrm{A}+\mathrm{B})}\right)\cdot\left(1-e^{-\mathrm{A}}\right)}$$

Therefore,

$$\lambda_{av}=\frac{\mathrm{A}}{2}\cdot\frac{1-e^{-2\mathrm{A}}}{\left(1-e^{-\mathrm{A}}\right)^2} \quad (14)$$

$$\lambda_{bv}=\frac{A\cdot(A+B)}{(2A+B)}\cdot\frac{1-e^{-(2A+B)}}{\left(1-e^{-(A+B)}\right)\cdot\left(1-e^{-A}\right)} \quad (15)$$

In order to decrease the number of model variables, it is worth relating the volume mean density in the RHS of Eq. (7) with the bulk mean density. Combination of Eqs. (10)–(12) leads to:

$$\frac{\rho_m-\rho_a}{\rho_{bm}-\rho_a}=\frac{\left(\rho_j-\rho_a\right)\cdot\phi_m}{\left(\rho_j-\rho_a\right)\cdot\phi_{bm}}=\frac{\phi_m}{\phi_{bm}} = \frac{(A+B)\cdot\left(1-e^{-B}\right)\cdot\left(1-e^{-A}\right)}{A\cdot B\cdot\left(1-e^{-(A+B)}\right)}=M \quad (16)$$

Finally, imposing for A and B the values of 2.77 and 2.025 respectively, the above parameters, $u_m/U_{\max}$,

ϕ_m/ϕ_{max}, λ_{av}, λ_{bv} and M assume the values of 0.338, 0.429, 1.571, 1.889, 0.701 correspondingly.

Re-arranging the previous Eqs. (1) and (5)–(8), it is possible to write:

- Expression for the entrainment:

$$U_e = E \cdot u_{max} = E \cdot \frac{A}{\left(1 - e^{-A}\right)} \cdot \quad u_m = I \cdot u_m \tag{17}$$

- Continuity equation:

$$\frac{d}{d\ell}\left(\rho_{bm} \cdot \pi R^2 \cdot u_m\right) = 2\pi R \cdot \rho_a \cdot U_e = 2\pi R \cdot \rho_a \cdot I \cdot u_m \tag{18}$$

- Momentum flux, *x*-direction:

$$\frac{d}{d\ell}\left\{\pi R^2 \left[\rho_a \lambda_{av} + \phi_{bm} \lambda_{bv}\left(\rho_j - \rho_a\right)\right] u_m^2 \cdot \cos\theta\right\} = 0 \tag{19}$$

- Momentum flux, *y*-direction:

$$\frac{d}{d\ell}\left\{\pi R^2 \left[\rho_a \lambda_{av} + \phi_{bm} \lambda_{bv}\left(\rho_j - \rho_a\right)\right] u_m^2 \cdot \sin\theta\right\} = -\pi R^2 \cdot \left(\rho_m - \rho_a\right) \cdot g = -\pi R^2 \cdot M\left(\rho_{bm} - \rho_a\right) \cdot g \tag{20}$$

- Integral jet fluid mass balance:

$$\phi_{bm} = \frac{Q_o \cdot \rho_j}{\pi R^2 \rho_j u_m} = \frac{Q_o}{\pi R^2 \cdot u_m} \tag{21}$$

In order to get a simpler set of ordinary differential equations, the above expressions (18)–(21) are differentiated and rearranged. In particular, Eqs. (19) and (20), after developing the derivative, are divided by cosθ and sinθ, respectively, and combined together by simply subtracting the LHS and RHS of Eq. (20) to the corre-sponding terms of Eq. (19), thus leading to Eq. (22). Furthermore, Eq. (21)is differentiated with respect to dℓ and substituted in Eq. (18) , finding a relation between (dR/dℓ) and (du_m/dℓ). This is then substituted in Eq. (19) leading to Eqs. (23) and (24): Eqs. (22)–(24) constitute the set of three ordinary differential equations to be solved to predict all jet features.

$$\frac{d\theta}{d\ell} = \frac{-M \cdot \phi_{bm} \cdot \left(\rho_j - \rho_a\right) \cdot g \cdot \cos\theta}{\left[\rho_a \lambda_{av} + \phi_{bm} \lambda_{bv}\left(\rho_j - \rho_a\right)\right] \cdot u_m^2} \tag{22}$$

$$\frac{du_m}{d\ell} = \frac{d\theta}{d\ell} \cdot u_m \cdot \tan\theta - \frac{2 \cdot \lambda_{av} \cdot \rho_a \cdot I \cdot u_m}{\left[\rho_a \lambda_{av} + \phi_{bm} \lambda_{bv}\left(\rho_j - \rho_a\right)\right] \cdot R} \tag{23}$$

$$\frac{dR}{d\ell} = \frac{1}{2 \cdot u_m} \cdot \left(2 \cdot I \cdot u_m - \frac{du_m}{d\ell} \cdot R\right) = \frac{1}{2 \cdot u_m} \cdot \left\{I \cdot \left[2 \cdot u_m + \frac{2 \cdot \lambda_{av} \cdot \rho_a \cdot u_m}{\left(\rho_a \lambda_{av} + \phi_{bm} \lambda_{bv}\left(\rho_j - \rho_a\right)\right)}\right] - R \cdot u_m \cdot \tan\theta \cdot \frac{d\theta}{d\ell}\right\} \tag{24}$$

The following boundary conditions are applied at $\ell = 5 \cdot d_o$; in fact, the jet region between $\ell = 0$ and $\ell = 5 \cdot d_o$ is known as the jet development region and is not considered here as its details do not affect the far away behaviour of the jet:

- $R = d_o/2$ (with d_o the nozzle diameter);
- $\theta = \theta_0$ (with θ_0 initial nozzle inclination);

$u_m = u_0$ (with u_0 equal to $\frac{Q_0}{\pi d_o^2 / 4}$);

$\phi = \phi_0$;

ρ_a = constant ambient density.

Eqs. (22)–(24) have been solved by a simple numerical integration algorithm, based on the Euler method, implemented in two commercial computer programs (Matlab® and Excel®). Relevant files are available to the reader as Open Access material upon request to the authors..

The numerical value of the discretization interval dℓ for the Euler method has to be chosen considering the length scale of the jet to be modelled. For all cases simulated in the present study, the value chosen for dl was 5×10^{-5} m because this value leads to sufficiently precise results in short computing times. Jet trajectory was computed on the basis of geometrical considerations, adding step by step a segment dl with a slope equal to the local angle θ.

2.3. Calibration of the entrainment coefficient E

The entrainment coefficient E is the only empirical parameter involved in the model, for which a value of 0.06 had previously been indicated [13] on the basis of comparisons between model predictions and experimental jet trajectories. In the present work a more detailed quantitative calibration of this parameter was

done by also considering experimental data from the literature [9,10,14], resulting in a slightly modified value of 0.058 that was employed throughout the present work.

As in all cases brine discharges were concerned, it is worth noting that the discharged stream density was computed as $\rho = \rho_w + kC$, where ρ_w = density of pure water [kg/m^3], C = salt concentration [kg/m^3] and k = 0.642 at 25°C (obtained by regression of the data reported in Weast [18]).

2.4. Dimensional analysis of model equations

Several mathematical and dimensional analysis of this system have been presented in the literature [5,14], in order to identify the main dependences, particularly focusing on the definition of non-dimensional numbers or parameters, thus giving to the set of equations a general validity for scaling up and down the results. In the above-mentioned works a densimetric Froude number [Eq. (29)] was defined as a replacement for the conventional Froude number [Eq. (28)], which apparently eliminated the dependence on any other variable characterizing the system. Moreover, all geometrical parameters (dimensionally lengths) were normalized by the nozzle diameter.

Interestingly the dimensional analysis carried out within the present work has confirmed the role of the densimetric Froude number, also highlighting some novelties of the present formulation. Starting from the above equations, the variables have been normalized as follows:

$$R^* = \frac{R}{d_0} \tag{25}$$

$$u_m^* = \frac{u_m}{u_0} \tag{26}$$

and the three dimensionless groups have been introduced:

$$\rho_j^* = \frac{\rho_j}{\rho_a} \quad \text{(densimetric ratio)} \tag{27}$$

$$Fr = \frac{u_0^2}{d_0 \cdot g} \quad \text{(conventional Froude number)} \tag{28}$$

$$Fr_{den} = \frac{u_0}{\sqrt{\left(\rho_j^* - 1\right) \cdot d_0 \cdot g}} \quad \text{(densimetric Froude number)} \tag{29}$$

For sake of brevity the algebraic steps are not reported, but the elaboration of Eqs. (18)–(21) leads to the following dimensionless equations:

- Continuity equation:

$$\frac{d}{dl^*}\left\{\left[1+\left(\rho_j^* - 1\right)\cdot\phi_{bm}\right]\cdot\pi R^{*2}\cdot u_m^*\right\} = 2\pi R^* \cdot I \cdot u_m^* \tag{30}$$

- Momentum flux, x-direction:

$$\frac{d}{dl^*}\left\{\left[\lambda_{av} + \phi_{bm}\lambda_{bv}\left(\rho_j^* - 1\right)\right]\cdot\pi R^{*2} u_m^{*2}\cdot\cos\theta\right\} = 0 \tag{31}$$

- Momentum flux, y-direction:

$$\begin{aligned}\frac{d}{dl^*}&\left\{\left[\lambda_{av} + \phi_{bm}\lambda_{bv}\left(\rho_j^* - 1\right)\right]\cdot\pi R^{*2} u_m^{*2}\cdot\sin\theta\right\} \\ &= \frac{d_0 g R^{*2}\cdot M}{u_o^2}\cdot\left(\rho^* - 1\right) \\ &= \frac{R^{*2}\cdot M}{Fr}\cdot\left[\phi_{bm}\left(\rho_j^* - 1\right)\right] = \frac{R^{*2}\cdot M\cdot\phi_{bm}}{Fr_{den}^2}\end{aligned} \tag{32}$$

- Integral jet fluid mass balance:

$$\phi_{bm} = \frac{\frac{\pi d_0^2}{4}\cdot u_0}{\pi R^2 \cdot u_m} = \frac{1}{4R^{*2}\cdot u_m^*} \tag{33}$$

Eqs. (30)–(32) highlight the dependence of model results on the Froude number and the densimetric ratio ρ_j^*. Notably, the introduction of the densimetric Froude number [Eq. (32)] in spite of the classical Froude number, causes the densimetric ratio ρ_j^* to disappear in the RHS of Eq. (32), though it still remains in the LHS of Eqs. (30)–(32). It should be observed, however, that the densimetric ratio ρ_j^* appearing in the LHS of Eqs. (30)–(32) is in all cases the least significant term of a sum. It can be inferred that, although the dependence of jet behaviour on the densimetric ratio ρ_j^* is almost entirely absorbed by the introduction of the densimetric Froude number, for large values of ρ_j^* a residual dependence on this parameter should be expected.

In order to highlight this finding, model predictions were used to analyse the trend of the normalized jet trajectory maximum, Y/d_0, as a function of both the classical Froude number (Fig. 2a) and the densimetric Froude number (Fig. 2b) for five different values of the densimetric ratio ρ_j^*.

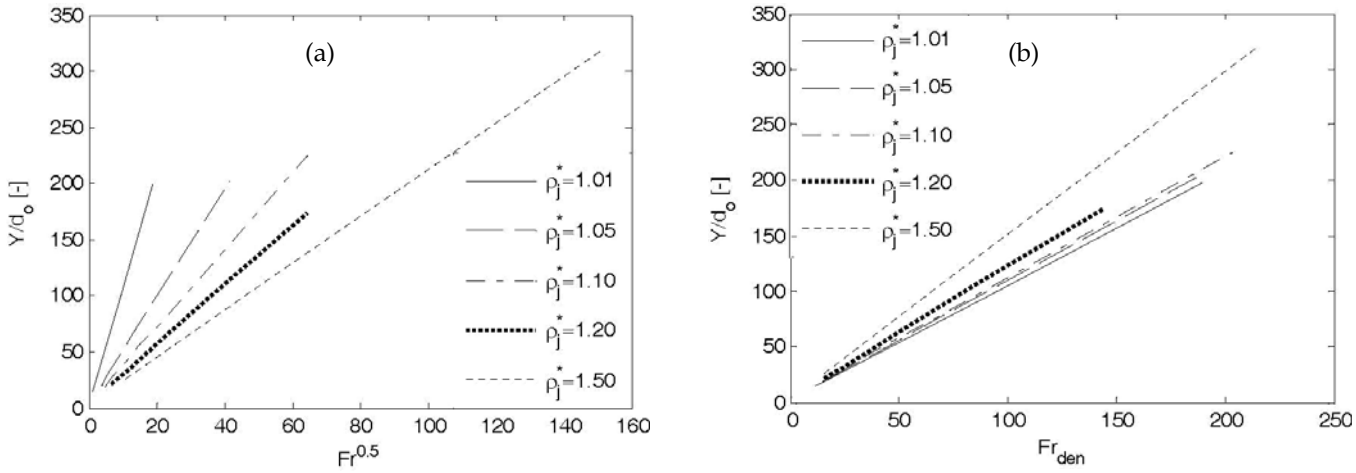

Fig. 2. Trend of the normalized jet trajectory maximum (Y/d_0) vs. $\sqrt{Fr}$ (a) and Fr_{den} (b) for 45° inclined dense jets with d_o varying from 1 to 4 mm, Q_0 varying from 0.1 to 2.0 L/min, and different values of ρ_j^* (ρ_j/ρ_a).

Clearly the choice of Fr_{den} reduces dramatically the dependence on ρ_j^* with respect to the use of Fr. Also, a residual dependence on ρ_j^* can be observed in Fig. 2b, in particular when density differences attain values of about 50%. It is worth noting however that when salty effluents are concerned, ρ_j^* typical values range from 1.0–1.06 (desalination plant effluents) to 1.2 (very concentrated brines), and for most practical uses the residual dependence on ρ_j^* can be neglected (Fig. 2b), leaving Fr_{den} as the sole significant correlating parameter. As a matter of fact, for the above values of the density differences the predicted residual dependence on ρ_j^* is smaller than experimental uncertainties, and has therefore been overlooked in experimental works so far [3,5,6,9–11].

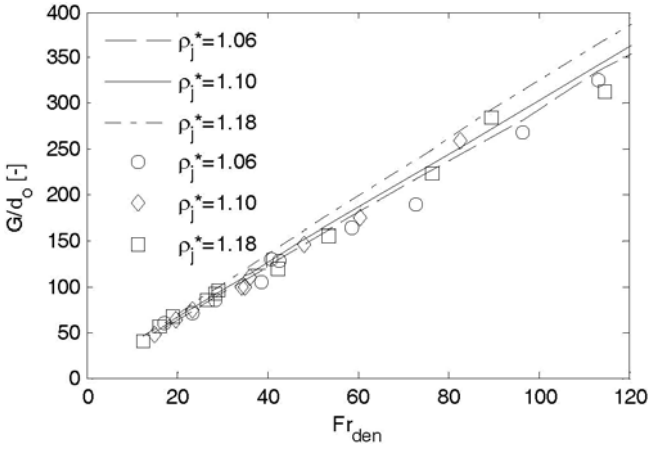

Fig. 3. Normalized return point distance for 45° inclined jets with d_o varying from 1 to 4 mm, Q_0 varying from 0.14 to 1.8 L/min and densimetric ratios of 1.06, 1.10, and 1.18. Symbols: experimental data from Cipollina et al. [10]. Lines: model predictions.

3. Model results

3.1. Return point distance

The return point distance is usually defined as the distance from jet nozzle at which the jet centreline returns to nozzle height. It coincides in practice with the impact point distance from jet nozzle in the case of horizontal seafloor and jet issuing from ground level, although with the simplifying assumption of neglecting possible effects of the seafloor in the jet behaviour. On the basis of the above dimensional analysis considerations, relevant experimental data from Cipollina et al. [10] for jets issuing at 45° have been plotted vs. the densimetric Froude number in Fig. 3. On the same figure model predictions are reported for comparison purposes, and a very good agreement can be observed.

At a closer inspection model predictions are found to only slightly depend on the densimetric ratio, as expected. Unfortunately the experimental data scatter does not allow confirming the slight dependence predicted. In any case, at this nozzle inclination the model appears to be sound, in view of the good agreement observed over the quite wide range of densimetric Froude numbers encompassed.

Similar results are obtained for jets issuing at 60° as can be observed in Fig. 4 where also a correlation by Roberts et al. [9] is reported as an alias of their experimental data. Fig. 4 shows that model predictions are also in very good agreement with the experiment at 60° nozzle inclination, which implies that the effects of nozzle inclination are well reproduced by the model. Also, the favourable comparison with other literature information may be regarded as a further confirmation of model soundness.

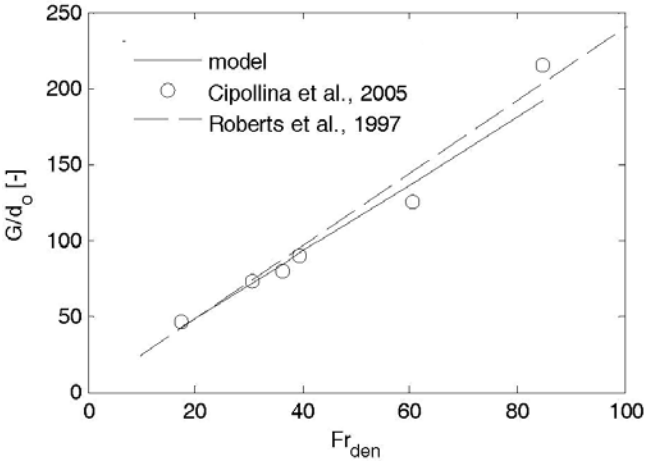

Fig. 4. Normalized return point distance for 60° inclined jets with d_o varying from 2 to 4 mm, Q_0 varying from 0.3 to 0.9 L/min and densimetric ratio of 1.10. Circles: experimental data from Cipollina et al. [10]. Solid line: model predictions. Dotted line: empirical correlation by Roberts et al. [9].

3.2. Centreline maximum

Another jet trajectory feature of interest is the centreline maximum. In Fig. 5 experimental data from Cipollina et al. [10] are compared with model predictions and once again a good agreement can be observed between the two, for both 45° and 60° inclined jets.

As regards the position of the centreline maximum coordinate on the horizontal axis, similar results are obtained, although the relevant figures are not reported for the sake of brevity. It can be concluded that jet trajectory is very well reproduced by the proposed model.

3.3. Maximum rise level

As concerns the maximum height attained by the upper edge of the jet, it is worth emphasizing that this is an ill-defined quantity, as no obvious dilution level can be assumed to correspond with the "visible" upper jet edge. It is, however, an important parameter, as in practical applications it is usually required that the jet boundary stays far away from water free surface.

If one assumed for the upper jet edge a distance of R for the jet centreline, then the visible maximum rise level would be over-predicted. It is worth noting, however, that, in addition to the difficulty in defining a suitable concentration level for the visible edge, the assumption of a Gaussian distribution of velocities and concentrations is quite an oversimplification of the real situation, as the density difference is bound to modify the symmetry of velocity and concentration distributions [14]. In particular, the presence of gravitational forces tends to dampen turbulent fluctuations at the upper boundary edge of the

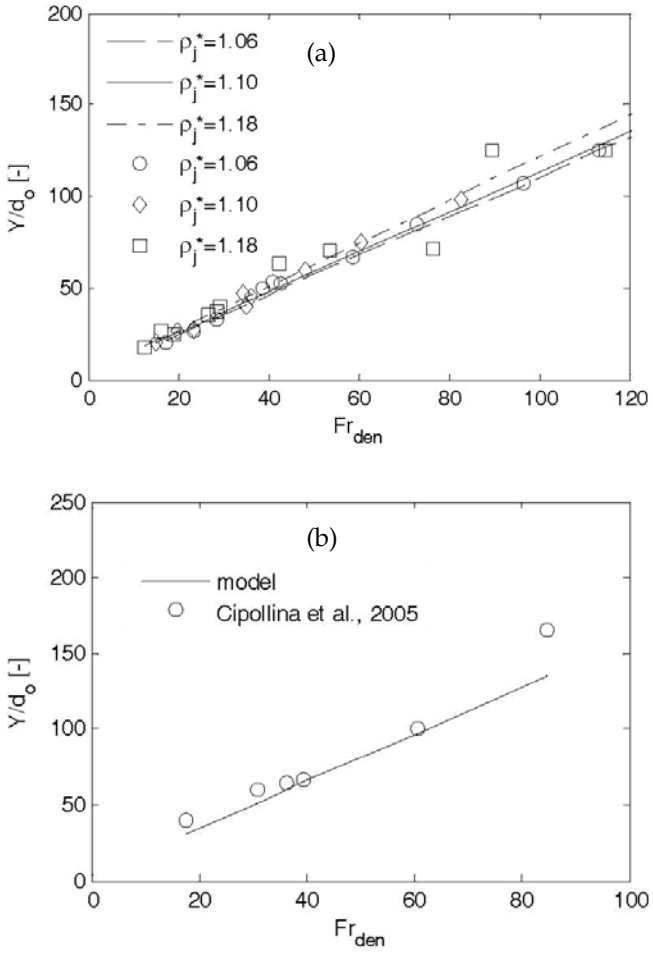

Fig. 5. Normalized trajectory centreline maximum. (a) 45° inclined jets with d_o varying from 1 to 4 mm, Q_0 varying from 0.14 to 1.8 L/min and densimetric ratios of 1.06, 1.10, and 1.18. Symbols: experimental data from Cipollina et al. [10]. Lines: model predictions. (b) 60° inclined jets with d_o varying from 2 to 4 mm, Q_0 varying from 0.3 to 0.9 L/min and densimetric ratio of 1.10. Circles: experimental data from Cipollina et al. [10]. Solid line: model predictions.

jet, where density gradients are negative in the upright direction. The upper jet edge is therefore neater and somewhat closer to the jet axis. On the contrary, density gradients tend to promote turbulence at the lower jet boundary, which is therefore enlarged and spread out by gravity. This results in a Gaussian profile distortion and a reduction of the experimentally detectable distance between the jet centreline maximum and the maximum rise level, as it may be observed in experimental dense jet images [14].

Given the above consideration, it has been observed that if the jet upper boundary is located at a distance $R/\sqrt{2}$, as done in other works [17,19], then a good agreement is found between model predictions and experiment, as shown in Figs. 6a and 6b.

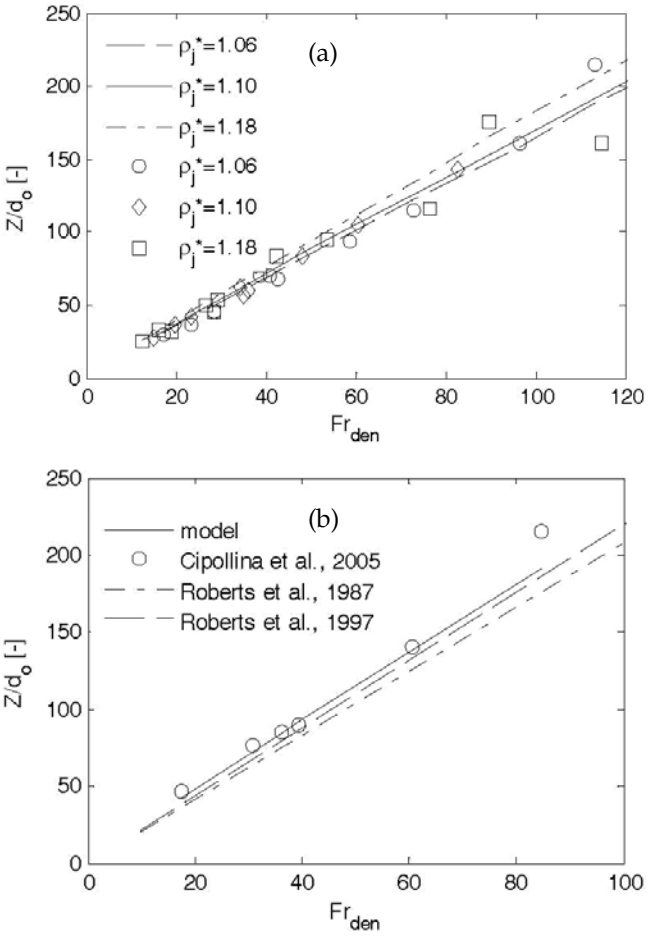

Fig. 6. Normalized maximum rise level. (a) 45° inclined jets with d_o varying from 1 to 4 mm, Q_0 varying from 0.14 to 1.8 L/min and densimetric ratios of 1.06, 1.10, and 1.18. Symbols: experimental data from Cipollina et al. [10]. Lines: model predictions. (b) 60° inclined jets with d_o varying from 2 to 4 mm, Q_0 varying from 0.3 to 0.9 L/min and densimetric ratio of 1.10. Circles: experimental data from Cipollina et al. [10]. Solid line: model predictions. Dotted line: empirical correlation by Roberts et al. [5,9].

Notably, although the model assumption of a symmetrical profile is clearly an oversimplification if jet boundaries are concerned, it may still have a limited impact on the trajectory centreline prediction, as the entrainment overestimation at the upper edge may well be counterbalanced by the entrainment underestimation at the lower edge.

3.4. Jet geometry summary

An alternative and possibly more effective way for comparing model predictions and experimental results may stem from the observation that simple proportionalities are found between jet features and densimetric Froude number, as observed in Figs. 3–6. A concise yet comprehensive model validation can therefore be obtained by directly comparing the following proportionality coefficients, both experimentally assessed and predicted by the model:

$$X/d_0 = \mathbf{k_X}\cdot \mathrm{Fr}_{\mathrm{den}} \quad (34)$$

$$Y/d_0 = \mathbf{k_Y}\cdot \mathrm{Fr}_{\mathrm{den}} \quad (35)$$

$$G/d_0 = \mathbf{k_G}\cdot \mathrm{Fr}_{\mathrm{den}} \quad (36)$$

$$Z/d_0 = \mathbf{k_Z}\cdot \mathrm{Fr}_{\mathrm{den}} \quad (37)$$

Such a comparison is made in Fig. 7 where model predictions are compared with experimental data from works both by Cipollina et al. [10] and Kikkert et al. [14]. The good agreement observed for all jet geometry features may be regarded as a complete validation of the model capability to predict jet geometry.

It is worth noting that for jets issuing with inclinations larger than 70° significant phenomena not included in the present model occur, namely the fall of the jet over itself that changes the jet environment and slows down its dilution rate. Clearly these phenomena are not accounted for by the present model, which should therefore be considered fairly accurate only for slopes not higher than 70°. Indeed, experimental information shows a decreasing trend of the maximum rise level when the initial inclination is higher than 70° [11].

3.5. Dilution at return point

Apart from jet geometry, other jet features are important for diffuser design, namely the dilution attained before returning to the nozzle height (practically the impact point) and return point velocity. As concerns the former, a comparison with experimental evidence is provided in Fig. 8 where model predictions of dilution attained at the above defined return point are plotted vs. an empirical correlation by Roberts et al. [9] (which may be regarded as an alias of their experimental data):

$$S_i = 1.6\cdot Fr_{den} \ (\pm 12\%) \quad (38)$$

where S_i is the centreline (minimum) dilution, achieved at the return point, defined as:

$$S_i = \frac{C_0}{C_{i,\max}} = \frac{1}{\phi_{i,\max}} \quad (39)$$

Once again, quite good agreement between model predictions and experimental values can be observed in Fig. 8 so that the capability of the present model to predict jet dilution may also be regarded as being validated.

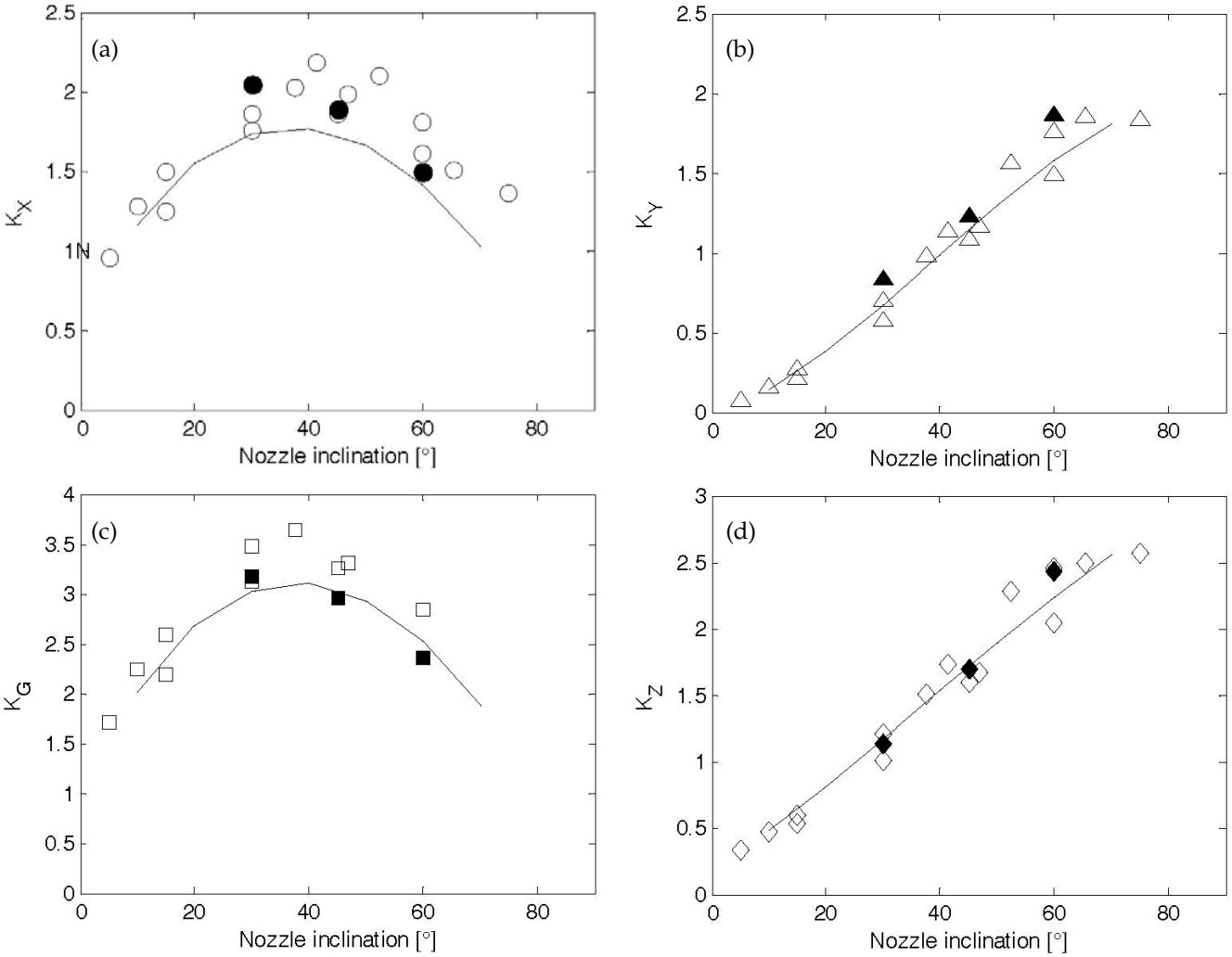

Fig. 7. Proportionality coefficients k_X (a), k_Y (b), k_G (c) and k_Z (d) vs. nozzle inclination. Solid symbols: experimental data from Cipollina et al. [10]. Empty symbols: experimental data from Kikkert et al. [14]. Solid lines: model predictions.

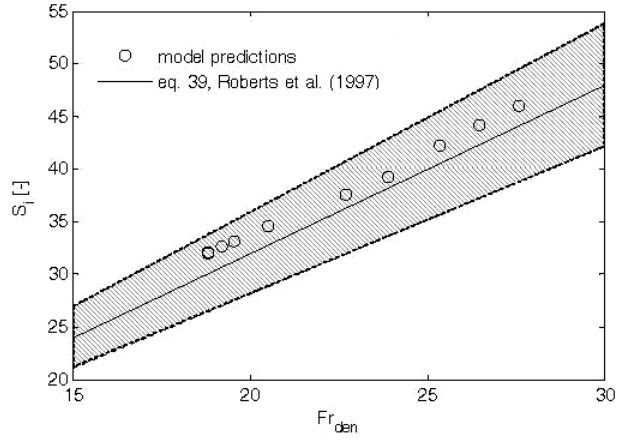

Fig. 8. Centreline (minimum) dilution at return point. Circles: dilutions predicted by the model at experimental conditions presented by Roberts et al. [9]. Solid line: empirical correlation presented by Roberts et al. [1]. Dashed lines: experimental error boundaries (±12%).

It can be noted that Roberts' experimental data were characterized by a jet initial salt concentration of about 50 g/L, with the exception of the two central points (C_0 = 28 and 33 g/L, respectively) whose predicted dilutions, indeed, seem to differ from the linear trend valid for all the other points. This underlines that the dilution at the return point also should be expected to present a dependence on the ρ_j/ρ_a ratio, although once again this is much less important than the dependence on the densimetric Froude number.

Another comparison has been made using experimental data presented by Kikkert et al. [14] concerning the integrated dilution measured by a light attenuation technique. Fig. 9 shows the trend of predicted and measured dilution values varying the nozzle inclination. Predicted integrated dilutions were calculated from centreline values according to the following equation, as suggested in [14]:

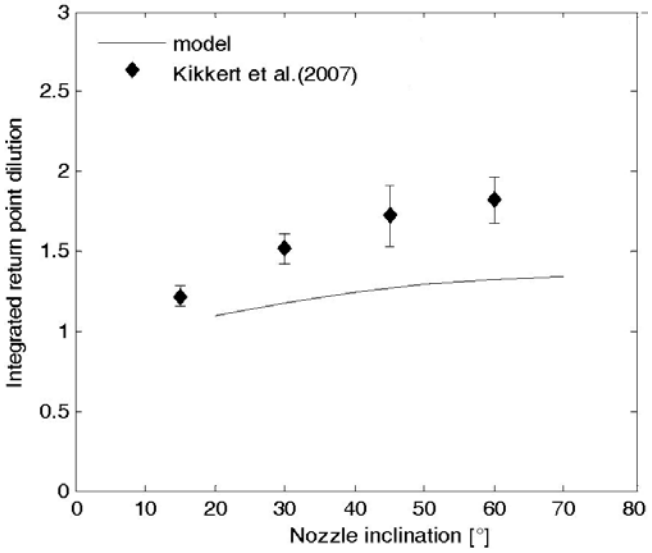

Fig. 9. Integrated dilution at return point vs. initial issuing angle. Comparison between model predictions and experimental data by Kikert et al. [14].

$$\text{integrated } S_i = \frac{S_i}{\sqrt{\pi}\frac{b_c}{d_0}} \tag{40}$$

where b_c corresponds to the jet spread where the local concentration drops to exp(−1) times the centreline value, and d_o is the nozzle diameter.

In this case, Fig. 9 shows a poorer agreement between model predictions and the experiment, indicating an underestimation of about 30% of the model in predicting return point dilutions in particular for the higher values of issuing inclination. This behaviour could be related to the simpler nature of the proposed model, which does not take into account any ground-boundary effects. In fact, the presence of turbulence promoted dilution at the impact point of the jet with the floor gives rise to higher dilutions than those predicted by the model at its "return point". Interestingly, also the analytical model developed by Kikkert et al. [14] showed a similar discrepancy between predictions and experiment, likely due to the similar simplifying assumptions used in their model formulation. However, the conservative behaviour of such predictions, along with the good comparison shown with results by Roberts in 1997 [9], allow for the use of the presented model for the estimation of jet dilutions in a preliminary design of brine discharge diffusers.

3.6. Return point velocities

Jet velocity at the impact point on the sea floor is an important design parameter, as it is on the basis of its value that the possible need for sea floor erosion countermeasures is assessed. Despite its importance as a design parameter, it has received very little attention so far. Although the model does not consider the interactions with solid boundaries (such as the sea floor), it is able to estimate jet velocities along the theoretical trajectory and therefore also on the centreline at the return point, i.e. at the point where the jet trajectory returns to the nozzle height. As no experimental information was retrieved in the open literature to validate these predictions, one might argue that having validated the model for all other jet features, it may be inferred that also for this important parameter the model should be expected to work. However, in order to provide a more direct validation, preliminary particle image velocimetry (PIV) data were obtained by means of a Dantec FlowMap PIV2000 processor, equipped with a HiSense PIV/PLIF double frame camera CCD 80C60 and a double cavity Nd:YAG Solo PIV pulsed laser. The investigated case was that of a jet issuing at 45°, with nozzle diameter of 2 mm, density ratio = 1.10, flow rate = 0.3 L/min. It is worth noting that with the double frame timing adopted only velocities smaller than 0.25 m/s were reliably measured.

The centreline velocities obtained are reported in Fig. 10 as solid symbols, together with present model predictions, and a very good agreement between the two can be observed. Thus, also for centreline velocities the model may be regarded as being well validated by comparison with experiment.

Having validated the model, it is interesting to predict return point velocities for various inclined jets and see whether once again a simple dependence on the densimetric Froude number is obtained. The model predictions obtained assuming nozzle diameters from 2 to 4 mm, density ratios from 1.1 to 1.2 and initial velocities from 0.5 to 6.0 m/s, have been reported as symbols in Fig. 11, where it can be observed that all data do align on a simple curve, practically regardless of the issuing angle.

The solid line reported on the same figure as a fitting curve is the following simple reverse proportionality:

$$\frac{u_{i,\max}}{u_0} = \frac{1.83}{Fr_{den}} \tag{41}$$

which reproduces very well all model predictions. Eq. (41) may therefore be employed for quick estimations of impact point velocity of dense inclined jets issuing from a slope-less sea floor, provided that $20° < \theta_0 < 70°$. In practice, positive deviations from Eq. (41) of about 10%, 25% and 60–70% are observed at issuing angles of 15°, 10° and 5° respectively, i.e. at θ_0. values unlikely to be adopted in real situations. This observation clearly implies that, as far as the velocity at impact point is concerned, the issuing angle cannot be regarded as a design parameter.

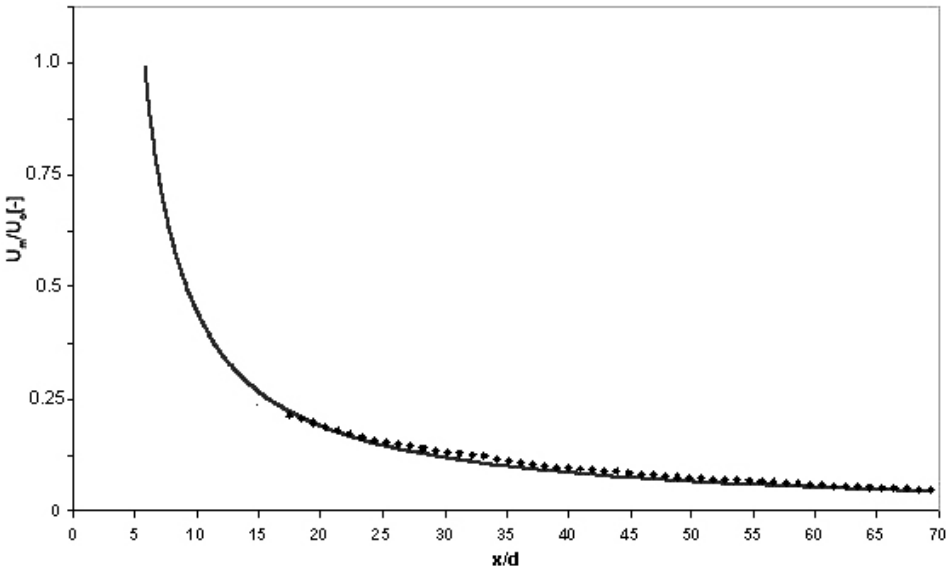

Fig. 10. Centreline velocity profile along the trajectory normalised by the nozzle diameter. Continuous line is the profile predicted by the model, dotted line is the PIV experimental profile. Q_0 = 0.3 L/min; d_o = 2 mm; ρ_j/ρ_a = 1.10; α= 45°.

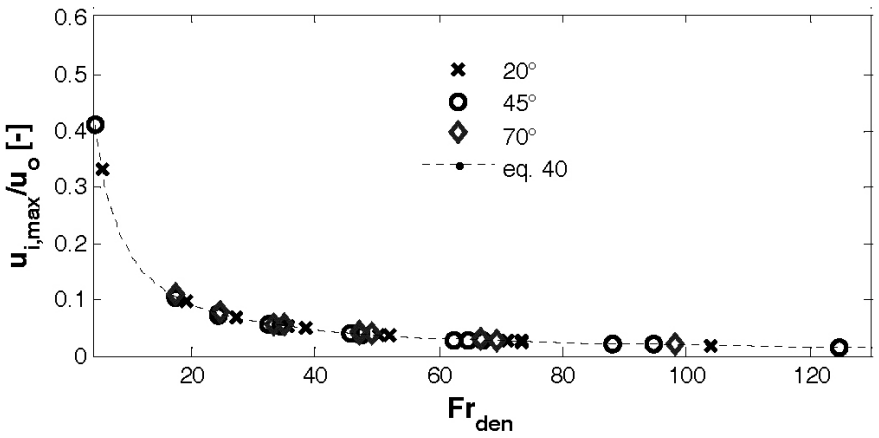

Fig. 11. Dependence of the centreline velocity at the return point with the densimetric Froude number for 20°, 45°, and 70° inclined dense jets ($u_{i,max}$ is the centreline velocity at the impact point, and it is normalised by the issuing velocity, u_0). Symbols: model predictions at different issuing jet conditions. Solid line: inverse proportionality law [Eq. (40)].

4. Using the implemented model

The model, implemented using a standard Excel® spreadsheet, is available for the reader in an easy-to-use form, which is also illustrated in the notes attached to the spreadsheet. In order to illustrate the reader how to use the implemented model, a short example is presented. Fig. 12 shows the flowsheet in which the user can insert jet characteristics and read the model predictions.

In this example, the model requires the specification of the jet by inserting only the following features in the white coloured cells:

- Issuing flow rate, Q = 1000 L/min;
- Initial density, ρ_0 = 1050 kg/m^3;
- Nozzle diameter, d_o = 80 mm;
- Nozzle inclination, α = 45°;
- Ambient density, ρ_a = 998 kg/m^3;

Moreover, a discretization step of 0.25 mm is chosen, and the simple case of flat seafloor is taken into account.

Numerical results are immediately available on the spread sheet itself. The return point is located where the trajectory passes through Y = 0. Along this line in the figure some crucial parameters are indicated by circles, e.g., the return point distance of 4.2 m, the return point mean velocity of 0.126 m/s, and the return point minimum dilution (on the centreline) of 27.8.

Fig. 13 shows a graphical representation of the jet geometry. In particular the central line represents the jet centreline trajectory; the upper and lower lines represent

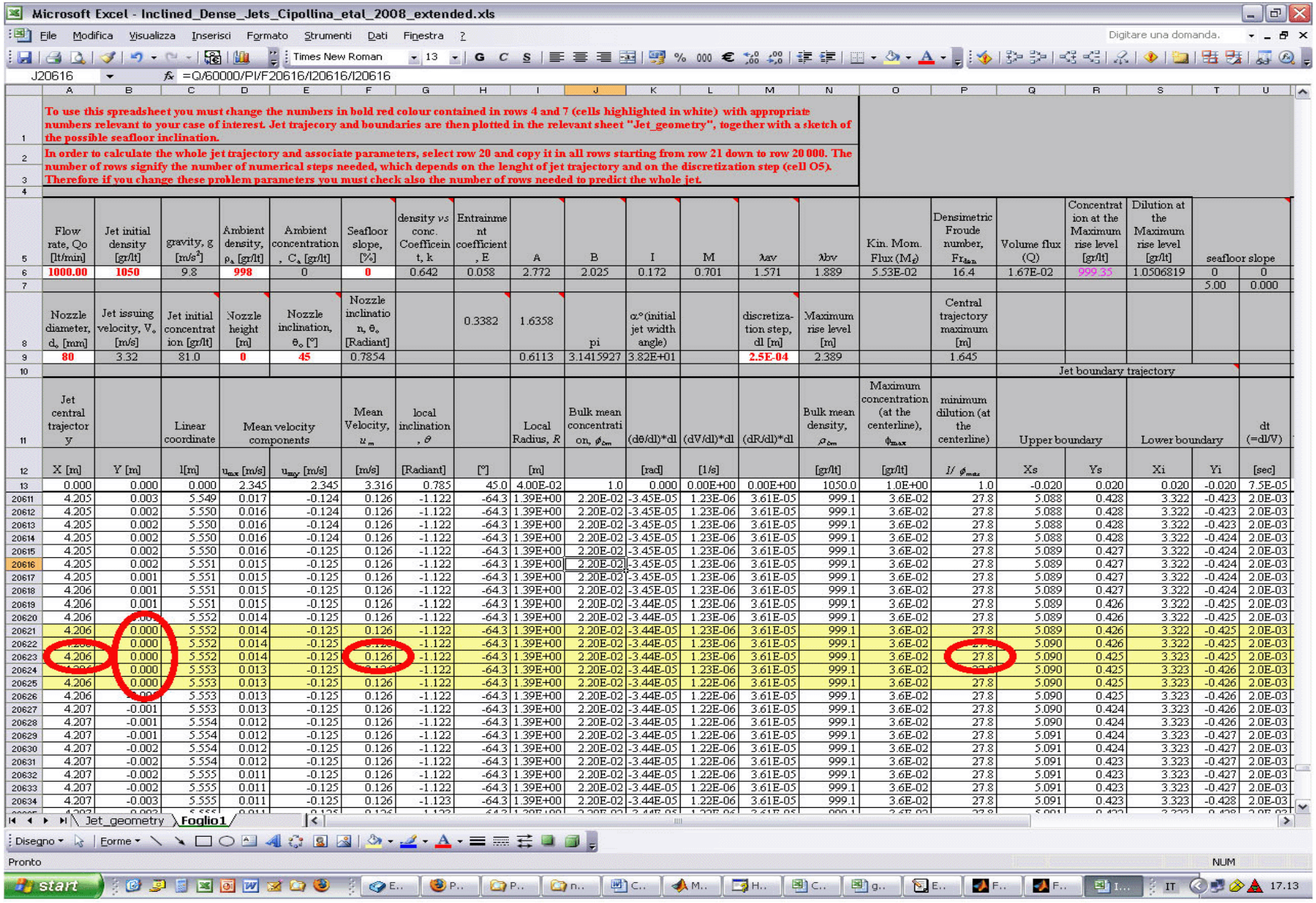

Fig. 12. Illustration of a part of the spread sheet where the model has been implemented.

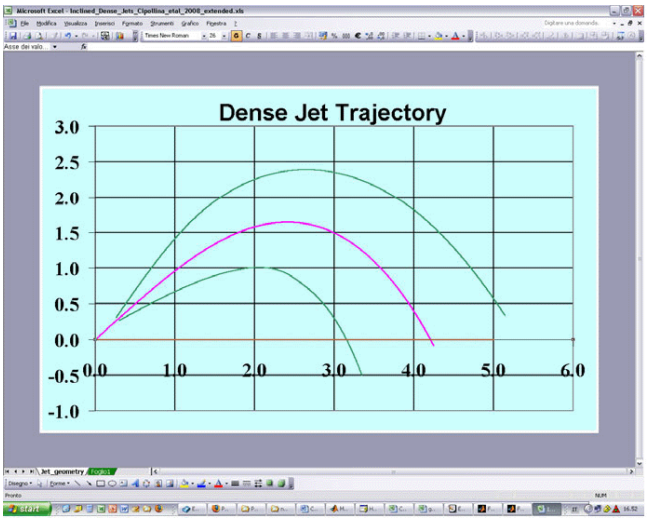

Fig. 13. Graphical representation of the geometry of a jet simulated using the spread sheet.

Thus, for example, the number, dimension, and inclination of the nozzles of an effluent diffuser could be first estimated by predicting several scenarios and analysing the possible different effects of the discharge on the sea environment. This would increase dramatically the knowledge of the problem, thus giving important indications for the planning of the accurate design of the effluent diffuser.

5. Conclusions

A simplified mathematical analysis of inclined dense jets has been performed in order to develop a model able to predict their behaviour. The model formulation takes into account physical variables which characterize the jet fluid dynamics (i.e. local velocities, local width of the jet, local inclination of jet trajectory and local dilution levels). The model is based on a set of ODAEs describing simple mass and momentum balances, which is easily solved by standard numerical methods.

Model predictions provide information on geometrical parameters (jet shape and axial trajectory geometry), on dilution levels achieved along the trajectory as well as on the velocity field that characterizes the jet.

Model predictions of all important jet features were validated by comparison with experimental data from various literature sources, or with original experimental information, and in all cases a good agreement was found.

An interesting result comes from a dimensional analysis of model equations, which confirmed the expectations that all dimensionless jet parameters mainly depend on the densimetric Froude number, though a weaker residual dependence on the densimetric ratio ρ_j/ρ_a. was found. This last is, however, so weak that, within the usual values of the densimetric ratio, it is overwhelmed by experimental error. As a consequence, for practical purposes, the Fr_{den} can normally be regarded as the sole important dimensionless parameter characterising dense jet behaviour. An experimental investigation conducted with very dense jets (i.e. with densimetric ratios significantly larger than 1.2) would be needed to assess whether the residual dependence on this last parameter predicted by the model is a real jet behaviour feature.

Notably, a novel feature of the model consists in also characterising the return velocity of the jet, finding once again a simple dependence (namely a reverse proportionality) on the densimetric Froude, which is reported for the first time to the authors' knowledge. Such data are of fundamental interest in order to assess possible erosion risks when discharging a salty effluent in the presence of a sandy floor.

Finally, electronic files for an easy use of the model are available for readers.

5. Symbols

b_c — Jet spread, m

C — Solute concentration (when jet density is related to a solute), kg/m^3

$C_{i,\max}$ — Jet axis solute concentration at return point (when jet density is related to a solute), kg/m^3

C_0 — Issuing jet solute concentration (when jet density is related to a solute), kg/m^3

$d\ell$ — Infinitesimal trajectory length (integrating interval), m

d_o — Nozzle orifice diameter, mm

dQ_e — Entrained infinitesimal flow rate through lateral surface, m^3/s

dS — Jet infinitesimal lateral surface = $2\pi R \cdot dl$, m^2

E — Entrainment coefficient = $U_e/u_{\max}$

Fr — Classical Froude number = $\dfrac{u_o^2}{g \cdot d_o}$

Fr_{den} — Densimetric Froude number = $\dfrac{u_o}{\sqrt{\dfrac{(\rho_j - \rho_a)}{\rho_a} \cdot g \cdot d_o}}$

F_s — Sinking force applied to the infinitesimal volume = $dV \cdot \Delta\rho \cdot g$, N

G — Distance of the return point of the jet on the nozzle horizontal, m

g — Gravity constant, =9.81 m/s^2

I — Averaged entrainment coefficient = U_e/u_m

k_G, k_z, k_x, k_y — Proportionality coefficients between normalized G, Z, X, Y and Fr_{den}

l — Linear jet coordinate, m
Q_0 — Initial jet flow rate, L/min
R — Conventional jet radius, m
r — Local radial distance from the axis, m
$u(r)$ — Punctual fluid velocity at a radial distance **r** from the axis, m/s
U_e — Entrainment velocity = dQ_e/dS, m/s
$u_{i,\max}$ — Jet axis velocity at the return point, m/s
u_m — Local mean velocity, m/s
$u_{\max}$ — Local jet axis velocity, m/s
u_0 — Issuing jet velocity = $Q_0/(\pi d_o^2/4)$, m/s
X,Y — Centreline maximum (trajectory maximum) coordinates taken from the source of the jet, m
Z — Ceiling level reached by the upper boundary of the jet, m

Greek

ρ_j^* — ρ_j/ρ_a = densimetric ratio, between issuing jet fluid and ambient fluid
ϕ_{bm} — Bulk mean jet volumetric fraction
$\phi(r)$ — Punctual jet volumetric fraction at a radial distance **r** from the axis
ϕ_m — Volume mean jet volumetric fraction
$\phi_{\max}$ — Local axis jet volumetric fraction
$\phi_{i,\max}$ — Local axis jet volumetric fraction at return point
θ — Local jet inclination above the horizontal plane, °
θ_o — Nozzle inclination above the horizontal plane, °
ρ_{bm} — Jet bulk mean density, kg/m^3
ρ_a — Ambient density, kg/m^3
ρ_j — Issuing jet density, kg/m^3
ρ_m — Jet volume mean density, kg/m^3

Acknowledgements

The authors wish to thank Prof. Salvatore Nicosia for the assistance throughout the work and Daniele Bellini for his contribution in collecting the PIV data. Prof. Mark Davidson and his group are gratefully acknowledged for providing us with the electronic version of their experimental data.

This research work was carried out with the financial support of the Italian Ministry of University and Research, D.M. n.720 14.12.99, *Piano Ambiente Terrestre*, Cluster 11B, Project No. 23 "ISR1".

References

[1] S. Lattemann and T. Hoepner, Seawater desalination impacts of brine and chemical discharge on the marine environment. Balaban, Rehovoth/L´Aquila/Davis, 2003.
[2] R. Einav, Environmental aspects of a desalination plant in Ashkelon. Desalination, 156 (2003) 79–85.
[3] J.S. Turner, Jets and plumes with negative or reversing buoyancy. J. Fluid Mech., 26 (1966) 779–792.
[4] W.P. James, I. Vergara and K. Kim, Dilution of a dense vertical jet. J. Environ. Eng. (ASCE), 124(6) (1983) 1273–1283.
[5] P.J.W. Roberts and G. Toms, Inclined dense jets in flowing current. J. Hydraulic Div. (ASCE), 113(3) (1987) 323–341.
[6] H. Zhang and E.R. Baddour, Maximum penetration of vertical round dense jets at small and large Froude numbers. J. Hydraulic Eng. (ASCE), 124(5) (1998) 550–553.
[7] F.M. Holly and J.H. Grace, Model study of dense jet in flowing fluid. J. Hydraulic Div. (ASCE), 98 (1972) 1921–1933.
[8] A.B. Pincince and E.J. List, Disposal of brine into an estuary. J. Water Poll. Control Fed., 45 (1973) 2335–2344.
[9] P.J.W. Roberts, A. Ferrier and G. Daviero, Mixing in inclined dense jets. J. Hydraulic Eng. (ASCE), 123(8) (1997) 693–699.
[10] A. Cipollina, A. Brucato, F. Grisafi and S. Nicosia, Bench scale investigation of inclined dense jets. J. Hydraulic Eng. ASCE, 131(11) (2005) 1017–1022.
[11] M.A. Zeitun, Conceptual design of outfall systems for desalination plants. Research and Development Progress Report No. 550, Office of Saline Water, US Department of Interior, as reported in Pincince and List (1973).
[12] L.N. Fan, Turbulent jets into stratified or flowing ambient fluids. Keck Laboratory of Hydraulics and Water Resources, California Institute of Technology, Report No.KH-R-15, 1967, as reported in N.P. Cheremisinoff, ed., Encyclopedia of Fluid Mechanics, Vol. 2, Gulf Publishing, Houston, 1986, pp. 440–441.
[13] A. Cipollina, A. Bonfiglio, G. Micale and A. Brucato, Dense jet modelling applied to the design of dense effluent diffusers. Desalination, 167 (2004) 459–468.
[14] G.A. Kikkert, M.J. Davidson and R.I. Nokes, Inclined negatively buoyant discharges. J. Hydraulic Eng. (ASCE) 133(5) (2007) 545–554.
[15] G.H. Jirka, Integral model for turbulent buoyant jets in unbounded stratified flows. Part I: single round jet. Environ. Fluid Mech., 4 (2004) 41–56.
[16] N. Rajaratnam, Turbulent mixing and diffusion of jets, in: N.P. Cheremisinoff, ed., Encyclopedia of Fluid Mechanics, Vol. 2, Gulf Publishing, Houston, 1986, pp. 391–400.
[17] G.H. Jirka, Improved discharge configurations for brine effluents from desalination plants. J. Hydraulic Eng. (ASCE), 134(1) (2008) 116–120.
[18] R.C. Weast, ed., Handbook of Chemistry and Physics, 56th ed., CRC Press, Cleveland, OH, 1975–1976.
[19] A.O. Demuren, in: N.P. Cheremisinoff, ed., Encyclopedia of Fluid Mechanics, Vol. 2, Gulf Publishing, Houston, 1986, pp. 440–441.